Am J Transl Res 2021;13(6):5796-5814
www.ajtr.org /ISSN:1943-8141/AJTR0129281

*Original Article*

# Osteoblast-activating peptide exhibits a specific distribution pattern in mouse ovary and may regulate ovarian steroids and local calcium levels

Ahmed E Noreldin[1,2], Mahmoud S Gewaily[3], Islam M Saadeldin[4], Mosleh M Abomughaid[5], Asmaa F Khafaga[6], Yaser H Elewa[7,8]

*[1]Department of Histology and Cytology, Faculty of Veterinary Medicine, Scientific Campus, Damanhour University, Damanhour 22511, Egypt; [2]Veterinary Anatomy, Faculty of Agriculture, Tottori University, Tottori, Japan; [3]Department of Anatomy and Embryology, Faculty of Veterinary Medicine, Kafrelsheikh University, Kafrelsheikh 33516, Egypt; [4]Department of Physiology, Faculty of Veterinary Medicine, Zagazig University, Zagazig 44519, Egypt; [5]Department of Medical Laboratory Sciences, College of Applied Medical Sciences, University of Bisha, Bisha 61922, Saudi Arabia; [6]Department of Pathology, Faculty of Veterinary Medicine, Alexandria University, Edfina 22758, Egypt; [7]Laboratory of Anatomy, Faculty of Veterinary Medicine, Basic Veterinary Sciences, Hokkaido University, Sapporo 060-0818, Japan; [8]Department of Histology, Faculty of Veterinary Medicine, Zagazig University, Zagazig 44519, Egypt*

Received December 29, 2020; Accepted May 6, 2021; Epub June 15, 2021; Published June 30, 2021

**Abstract:** Osteoblast-activating peptide (OBAP) is a novel protein affecting osteoblast proliferation and differentiation, but its ovarian expression is yet to be reported. Osteoporosis is a common disease, caused mainly by low estrogen levels in females. We investigated whether OBAP regulates estrogen synthesis and osteoporosis. Using immunohistochemical analyses, we studied the distribution of OBAP in different parts of the mouse ovary. We also attempted to clarify the correlation of OBAP with ovarian steroids and calcium-regulating factors in the same ovarian tissues, including aromatase (CYP19), 3β-hydroxysteroid dehydrogenase (3β-HSD), estrogen receptor (ER), progesterone receptor (PR), receptor activator of nuclear factor-κB (RANK), calmodulin, calbindin, and calcium-sensing receptor. The ovarian interstitial endocrine cells (IC) showed the greatest localization of OBAP, followed by the mature corpus luteum and the oocytes of mature Graafian follicles (MGF), while there were strong negative correlations of OBAP with CYP19. Strong positive correlations with 3β-HSD (except MGF), RANK (except IC), and calmodulin (except MGF and IC) were demonstrated. OBAP also showed partially positive correlations with ER and PR in the corpus luteum and with IC and calbindin in the MGF. We conclude that OBAP might be related to estrogen synthesis and calcium homeostasis.

**Keywords:** Ovary, OBAP, estrogen, calcium homeostasis, immunohistochemistry

## Introduction

Osteoporosis is a bone disease that mainly manifests in the elderly [1]. It is characterized by altered bone micro-architecture, bone demineralization, and bone damage. Osteoporosis results in over nine million fractures per year worldwide and causes serious economic, social, clinical and public health problems [2]. In developed countries, hip fractures are associated with 30% and 40% mortality rates in the first and second years, respectively, after fracture [3]. Fragility fractures are the cause of 1% of disabilities globally [4].

The leading cause of osteoporosis is elevated bone degradation and decreased bone synthesis [5]. The low production of estrogen from the ovaries in old age causes osteoporosis [6]. Osteoporosis can also be induced by ovariectomy in adult females [7], with a lack of estrogen potentially being the main result of an ovariectomy. D'Amelio, et al. [8] concluded that estrogen deficiency enhances osteoclast synthesis by elevating the number of osteoclast precursors because of the high production of receptor activator of nuclear factor-κB ligand (RANKL) and tumor necrosis factor-alpha (TNF-α).

Dick, et al. [9] proposed that a lack of estrogen in older women exacerbates renal calcium deficiency, thereby enhancing bone resorption. Moreover, the ovary has been reported to play a

pivotal role in calcium hemostasis via progesterone and estrogen hormones [10]. Estrogen elevates blood calcium levels by elevating serum 1,25(OH)2D and calcium absorption [11], whereas progesterone lowers calcium in the blood [12].

The aromatase enzyme, encoded by *CYP19a1*, synthesizes estrogens and is expressed at preovulatory follicles and large antral healthy follicles [13]. Aromatase is expressed most strongly in granulosa cells at the outer edge of the antral follicles, exceeding the levels of expression found in granulosa cells near the antral cavity [14, 15]. In rats, mature follicles at proestrus highly express aromatase in the granulosa layer [16].

Seifert-Klauss and Prior [17] noted that progesterone enhances bone building in peri- and premenopausal women, so the combination of antiresorptive effects with progesterone may increase bone formation. During the luteal phase, elevated progesterone relative to estrogen might be the main cause of low serum calcium levels [18]. Ishida and Heersche [19] suggested that progesterone enhances the differentiation and proliferation of osteoprogenitor cells in adult female rats, but not in adult male rats. Moreover, Wang, et al. [20] revealed that progesterone prevents osteoblast apoptosis by the downstream mitochondrial pathway and progesterone receptors (PRs). Therefore, progesterone may play a role in bone formation. Davey and Morris [21] suggested that combined treatment with estradiol and DHT enhanced early-phase osteoblast development when alkaline phosphatase is detected. Moreover, Westerlind, et al. [22] suggested that the rate of bone turnover is regulated by estrogen.

RANK (receptor activator of nuclear factor-κB) is a cytokine activated by RANKL, regulating bone metabolism and controlling the tumor immune response [23]. Postmenopausal osteoporosis is associated with an increased rate of bone remodeling, which leads to accelerated bone loss and increased risk of fracture. Bone resorption is dependent on RANKL, a TNF family member that is essential for osteoclast formation and activity. The catabolic effects of RANKL are prevented by osteoprotegerin (OPG), a TNF receptor family member that binds RANKL and prevents the activation of its single similar receptor, RANK, which is found on osteoclasts and preosteoclast precursors [24]. RANK-RANKL interactions lead to preosteoclast cell recruitment, fusion into multinucleated osteoclasts, and osteoclast activation and survival. RANK-mediated responses can be inhibited completely by OPG [24]. OPG is a secreted protein that is detectable in the peripheral circulation, where it binds to RANKL [24]. Cell culture studies showed a positive effect of estrogen [25, 26] on OPG production by human osteoblastic cells.

Calmodulin is one of the most common $Ca^{2+}$-binding proteins, playing a pivotal role in the transduction of various physiological responses [27]. Calmodulin mRNA is expressed in the ovary of virgin, pregnant, and postpartum mice and has been found in mouse tissues that support pregnancy, such as the uterus, decidua, and placenta [27]. Calbindin-D28k (CaBP28k) is a cytosolic calcium ($Ca^{2+}$)-binding protein expressed in the intestine, kidney, and placenta that mediates $Ca^{2+}$ homeostasis and is influenced by 1,25-dihydroxyvitamin D3 [28]. It is expressed abundantly in the immature mouse uterus and oviduct, where its immunoreactivity is restricted to the endometrial and glandular epithelium of both the uterus and the oviduct. CaBP28k is decreased markedly in the uterus but not in the oviductal epithelium at sexual maturity; this pattern continues in pregnant mice. Estrogen was also shown to decrease calbindin-D28k mRNA in the uterus but not in the oviduct, suggesting its effect on mammalian CaBP28k expression [29]. It is also expressed in the germinal epithelium and cells surrounding the oogonia and oocytes of developing and growing ovaries of chicken embryos, reflecting its crucial role during the early phases of oogenesis [30].

The calcium-sensing receptors (CaSRs) are transmembrane G-protein-coupled receptors that act as sensors responsible for modulating parathormone and calcitonin release in response to changes in blood calcium levels [31]. The CaSRs are considered the molecular basis for detecting the response of specialized cells to changes in the extracellular $Ca^{2+}$ concentration. The activation of these receptors triggers signaling pathways that modify many

cell functions [32]. The sensitivity of CaSRs in the epithelial cells on the ovarian surface to the extracellular $Ca^{2+}$ concentration can shift the cellular behavior from proliferation to irreversible differentiation or latency [33].

Recently, numerous antiresorptive agents have been used to treat osteoporosis, but the only accepted bone anabolic treatments are truncated and full-length parathyroid hormone [34]. In the rat stomach, Fukushima, et al. [35] detected a new anabolic peptide called the osteoblast-activating peptide (OBAP), which enhances the expression of various osteoblast differentiation markers [35]. Interestingly, OBAP is localized in the distal convoluted tubules of the mouse kidney [36] and parietal cells of the rat stomach [37], and is reported to have a direct relationship with calcium hemostasis and osteoporosis [38, 39]. In this context, we asked whether OBAP could play a role in calcium hemostasis in these organs, assuming that there are relationships between OBAP, ovarian steroid hormones, and calcium-controlling elements. We studied the ovarian distribution of OBAP to determine its role in calcium hemostasis and its relationship with the secreted ovarian hormones that contribute to bone formation.

## Materials and methods

### *Animals and tissue preparation*

Our studies were performed according to the NIH Guidelines for the Use and Care of Laboratory Animals and were approved by the Ethics Animal Care Committee of Tottori University, Japan (Approval No. 13-T-19). Twelve 9-week-old female BALB/cAJc1 mice (21-25 g; Shimizu Kagaku, Kyoto, Japan) were used in this study. After determining various estrous cycle stages using vaginal swabs [40], the animals were exposed to ether inhalation and euthanized by cervical dislocation. The ovaries were dissected and preserved in 4% paraformaldehyde in 0.1 M phosphate buffer overnight at 4°C for immunofluorescence (IF) and immunohistochemistry (IHC) studies.

### *Antibodies*

All antibodies, sources, working dilutions, and methods for antigen retrieval are presented in **Table 1**. The immunospecific reaction of anti-OBAP antibody was confirmed in the supplementary data provided by Noreldin et al. [37].

### *General routine staining and immunohistochemistry*

Briefly, 4-µm-thick paraffin sections were deparaffinized with xylene and rehydrated in graded alcohol. Some sections were stained with hematoxylin and eosin [41]. Other sections were subjected to antigen retrieval according to the type of antibody shown in **Table 1**. Next, the sections were immersed in 0.5% TritonX-100 (Nacalai, Kyoto, Japan) in phosphate-buffered saline (PBS) for 20 min, followed by 3% hydrogen peroxide in methanol for 5 min at room temperature to block endogenous peroxidase signals. The sections were blocked with 5% bovine serum albumin (Cat. #A9647; Sigma-Aldrich) diluted in 0.1 M PBS (pH 7.2) for 1 h. The incubation with primary antibodies was performed overnight at 4°C. In the negative control sections, normal immunoglobulin G (IgG) was substituted for the primary antibodies at the same concentration and antibody species. After washing, the sections were incubated with biotinylated IgG antiserum (Histofine kit; Nichirei, Tokyo, Japan) for 30 min at room temperature. Then, the sections were incubated with streptavidin-peroxidase conjugate for 30 min at room temperature. The detection of antibody-streptavidin-biotin complexes was performed using peroxidase/3,3-diaminobenzidine (Peroxidase/DAB ChemMate Detection Kit, Cat. #K5007; Dako, Real Carpinteria, CA, USA). Nuclear counterstaining was performed with Mayer's hematoxylin. Representative micrographs were captured under a microscope (IX71; Olympus, Tokyo, Japan) linked to a digital camera (DP-71; Olympus).

### *Immunofluorescence*

For IF analysis, the ovarian sections were first washed with 0.5% TritonX-100 and then treated with donkey serum (Cat. #GTX30972; GeneTex, Irvine, CA, USA) for 30 min. After that, the sections were incubated with the combination of specific primary antibodies reported in **Table 1** at 4°C overnight. The next day, the sections were treated with Alexa-Fluor-546-labeled donkey anti-rabbit IgG (1:200, Cat. #NL006; Invitrogen), Alexa-Fluor-488-labeled donkey anti-goat IgG (1:200, Cat. #NL001; Invitrogen,

**Table 1.** List of antibodies, sources, working dilutions, and methods of antigen retrieval

| Antibody | Source | Dilution | Antigen retrieval | Heating condition | References |
|---|---|---|---|---|---|
| Rabbit polyclonal anti-OBAP | (Processed on demand, Operon Biotechnologies, Tokyo, Japan) | 1:500 for IF and 1:800 for IHC | No | No | [37] |
| Goat polyclonal anti-PCNA | (sc-9857, Santa Cruz, CA, USA) | 1:2000 | 10 mM citrate buffer (pH 6.0) | 95°C, 20 min | [74] |
| Rabbit polyclonal anti-single strand DNA (SSDNA) | (A4506, Dako, USA) | 1:500 | No | No | [75] |
| Mouse monoclonal anti-CYP19 | (sc-374176, Santa Cruz, CA, USA) | 1:300 | No | No | [53] |
| Mouse monoclonal anti-3β-HSD | (sc-515120, Santa Cruz, CA, USA) | 1:200 | No | No | [57] |
| Mouse monoclonal anti-ER α | (sc-8005, Santa Cruz, CA, USA) | 1:400 | No | No | [76] |
| Mouse monoclonal anti-PR | (sc-810, Santa Cruz, CA, USA) | 1:300 | No | No | [77] |
| Rabbit polyclonal anti-RANK | (sc-9072, Santa Cruz, CA, USA) | 1:100 | No | No | -- |
| Rabbit monoclonal anti-calmodulin | (BS9898M, Bioworld Technology, Minneapolis, Minnesota, USA) | 1:300 | 10 mM citrate buffer (pH 6.0) | 105°C, 20 min | -- |
| Rabbit polyclonal anti-calbindin antibody | (E10340, Spring Bioscience, Pleasanton, CA, USA) | 1:500 | 10 mM citrate buffer (pH 6.0) | 105°C, 20 min | [78] |
| Mouse monoclonal anti-CaSR | (sc-47741, Santa Cruz, CA, USA) | 1:200 | No | No | [9] |

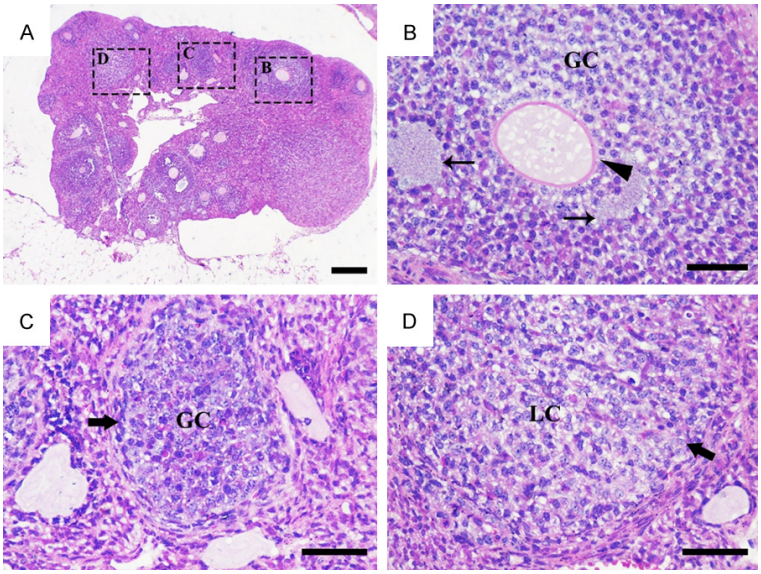


**Figure 1.** Normal histology of the diestrus mouse ovary. (A) Light micrograph of ovary revealing different developed ovarian follicles. (B) An inset of (A), showing an oocyte surrounded by the zona pellucida (arrowhead). Many liquor folliculi (arrows) are distributed between deeply basophilic stained granulosa cells (GC). (C) An inset of (A), revealing that the immature corpus luteum (arrow) has highly basophilic granulosa cells (GC). (D) An inset of (A), displaying the mature corpus luteum with lightly acidophilic stained luteal cells (LC). Scale bar = 200 μm.

Eugene, OR, USA), or Alexa-Fluor-488-labeled donkey anti-mouse IgG (Red: Cat. #NL007, lot: LZM1314091; Green: Cat. #NL009, lot: LZN-0711081), according to the species of raised primary antibody. Nuclei were counterstained with Hoechst 33342 (1:10,000, Cat. #H3570; Invitrogen, Eugene, OR, USA). The stained sections were examined with an Ix71 microscope (Olympus).

*Morphometry*

Four ovaries at each stage of the ovarian cycle were used for morphometry. Three representative levels of the whole ovary were cross-sectioned at 100 μm intervals, and three serial sections were obtained at each level. After IF staining, the whole ovary was captured at 4× magnification, and the photos were converted into grayscale. The integrated densities of OBAP-positive areas were measured using Image J (v1.46r; NIH, Bethesda, MD, USA) [42]. Differences in OBAP, calbindin, estrogen receptor alpha (ER-α), PR, calmodulin, RANK, 3β-hydroxysteroid dehydrogenase (3β-HSD), CaSR, and aromatase (CYP19) localization between whole ovaries and different parts of the ovaries obtained at each stage were explained as the variations in the integrated densities [43]. The single-stranded DNA (ssDNA) and proliferating cell nuclear antigen (PCNA) immunoreactivity was measured by the number of positive nuclei per $mm^2$ [43].

*Statistical analyses*

The data were analyzed by analysis of variance using SAS software SAS [44], and Duncan's new multiple range test was used to test for significance. Results are presented as the mean ± standard error (SE). Differences between means were considered significant at $P < 0.05$. Pearson's linear correlation coefficient was calculated to determine the correlation (R) between the mean expression of different proteins in the ovary (OBAP, PCNA, SSDNA, CYP19, 3β-HSD, ER-α, PR, RANK, Calbindin, Calmodulin, and CaSR), with R values > ±0.7 considered to represent a strongly positive/negative linear relationship, and R values < ±0.5 a weakly positive/negative linear relationship [45].

## Results

The mouse ovary comprises various developing follicles with endocrine interstitial cells between them (**Figure 1A**). Directly before ovulation, the oocyte is surrounded by the zona pellucida that is, in turn, surrounded by deeply basophilic granulosa cells to form the mature Graafian follicle (**Figure 1B**). After ovulation, the immature corpus luteum forms deeply basophilic granulosa cells without an oocyte (**Figure 1C**). The corpus luteum matures with lipochrome pigment accumulation, so the granulosa cells turn into faint acidophilic lutein cells (**Figure 1D**).

OBAP-positive cells were detected in the endocrine interstitial cells and oocytes of mature Graafian follicles, but granulosa cells were negative for OBAP (**Figure 2A-C**). The OBAP-positive cells were observed in the peripheral area of

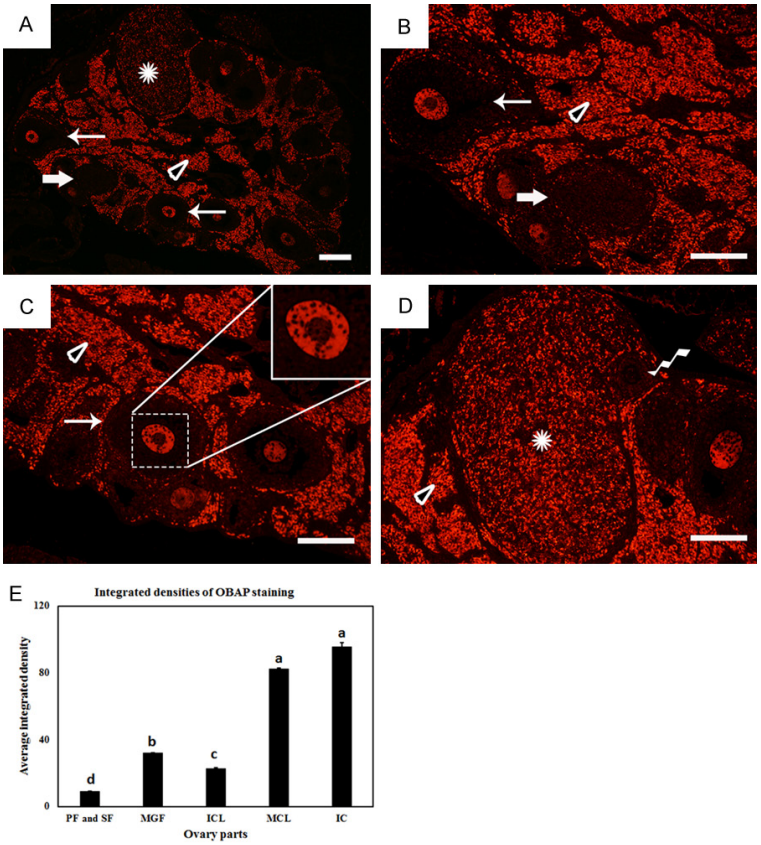


**Figure 2.** Distribution of osteoblast-activating peptide (OBAP)-immunopositive cells in the diestrus mouse ovary. (A) Immunofluorescence localization of OBAP revealing the reaction of different parts of the ovary with OBAP. (B-D) Insets of (A), showing the negativity for OBAP in the granulosa cells of mature Graafian follicle but positivity in the oocyte (thin arrows). Moreover, a strong OBAP reaction by endocrine interstitial cells was observed (arrowheads). The immature corpus luteum displays negativity for OBAP (thick arrows). On the other hand, the mature corpus luteum shows a moderately OBAP-positive reaction (asterisks). A negative OBAP reaction was seen in the primary follicle, even its oocyte (bent line). Some OBAP-immunopositive cells could be seen at the periphery of the mature Graafian follicle and immature corpus luteum, which might involve thecal cells. Scale bar = 200 μm. (E) Average integrated densities of OBAP staining for different parts of the ovary. Data are expressed as the mean ± SE. Bars with different superscripts are significantly different (Duncan's new multiple range test was used to compare the means among treatments; $P < 0.05$). PF, primary follicle; SF, secondary follicle; MGF, mature Graafian follicle; MCL, mature corpus luteum; ICL, immature corpus luteum; IC, interstitial cell.

the immature corpus luteum, with a negative reaction in the majority of the immature corpus luteum (**Figure 2B**). The reaction of OBAP within the oocyte was extensive in the ooplasm, except for tiny dots and the nucleus (**Figure 2C**). Some OBAP-immunopositive cells were seen at the periphery of the mature Graafian follicle and the immature corpus luteum, which might have been thecal cells (**Figure 2B** and **2C**). The mature corpus luteum (MCL) was filled with OBAP-positive cells (**Figure 2D**). The average integrated densities of OBAP staining in various parts of the ovary were markedly lower in the primary and secondary follicles and immature corpus luteum, followed by the mature Graafian follicle (**Figure 2E**). Meanwhile, the highest integrated densities of OBAP staining were observed in the endocrine interstitial cells, followed by the MCL (**Figure 2E**).

The different stages of estrous cycle of mouse was revealed in the Supplementary Figure 1. The number of OBAP-positive cells was high in proestrus (**Figure 3A**), decreased in estrus (**Figure 3B**), and then rose gradually in metestrus (**Figure 3C**) to reach the highest number in diestrus (**Figure 3D**). Interestingly, the average integrated densities of OBAP staining in different phases of the estrous cycle were significantly lower in the estrus phase than those in proestrus, metestrus, and diestrus ($P < 0.05$) (**Figure 3E**). The level of OBAP in the ovary was initially high in proestrus, then declined to the lowest level in estrus, after which it returned to a higher level in metestrus to reach its peak in diestrus.

We also measured the number of PCNA-immunopositive nuclei in each region of the ovary to determine the relationship between OBAP expression and the various developmental stages of ovarian follicles (**Figure 4A**). An abundance of PCNA-positive nuclei was detected in the mature Graafian follicle and immature corpus luteum (**Figure 4B** and **4C**). The MCL contained a small number of PCNA-positive nuclei (**Figure 4D**). The fewest PCNA-positive nuclei were observed in the interstitial cells (**Figure 4A-D**). The average number of PCNA-immunopositive nuclei peaked in the pri-

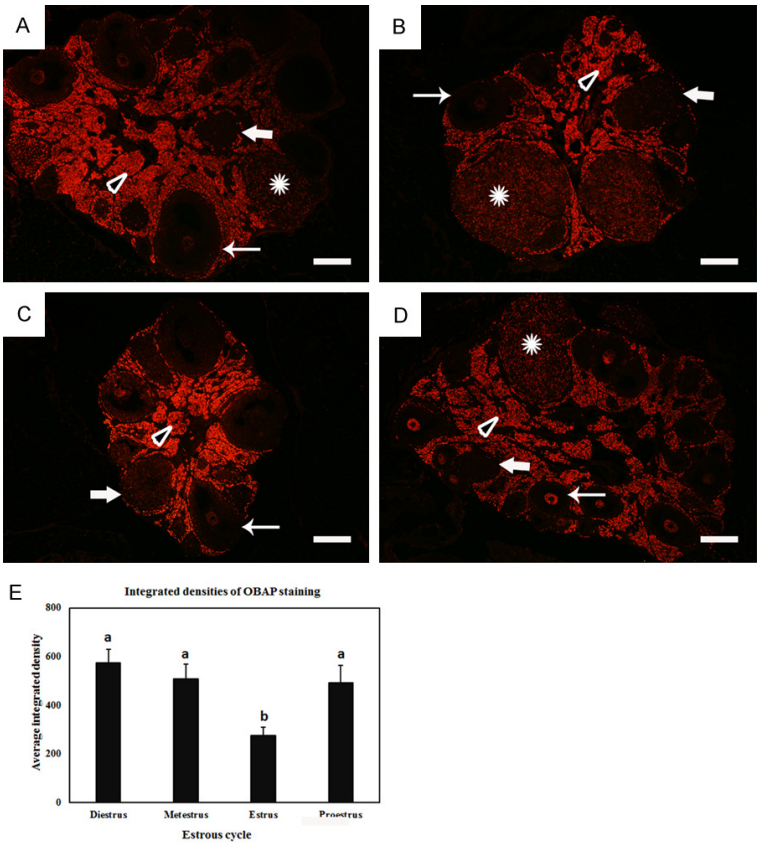


**Figure 3.** Distribution of osteoblast-activating peptide (OBAP)-immunopositive cells in different mouse ovarian estrous stages: (A) proestrus; (B) estrus; (C) metestrus; and (D) diestrus. Endocrine interstitial cells (arrowheads), mature corpus luteum (asterisks), immature corpus luteum (thick arrows), mature Graafian follicle (thin arrows). Scale bar = 200 μm. (E) Average integrated densities of OBAP staining for various stages of the estrous cycle. Data are expressed as the mean ± SE. Bars with different superscripts are significantly different (Duncan's new multiple range test was used to compare the means among treatments; $P < 0.05$). PF, primary follicle; SF, secondary follicle; MGF, mature Graafian follicle; MCL, mature corpus luteum; ICL, immature corpus luteum; IC, interstitial cell.

mary and secondary follicles and mature Graafian follicles, followed by the immature corpus luteum and then the MCL, whereas the lowest PCNA staining was observed in endocrine interstitial cells (**Figure 4E**).

We next investigated the relationship between OBAP expression and the stages of ovarian follicle development by observing the number of ssDNA-positive nuclei in different parts of the ovary (**Figure 5A**). ssDNA-positive nuclei were rarely observed in the mature Graafian follicle and immature corpus luteum (**Figure 5B** and **5C**), and a large number of ssDNA-positive nuclei were detected in the MCL (**Figure 5D**). The interstitial cells contained few ssDNA-positive nuclei (**Figure 5A-D**). The largest number of ssDNA-positive nuclei was detected in the MCL, whereas the lowest was in the primary and secondary follicles, along with the mature Graafian follicle and immature corpus luteum (**Figure 5E**).

IF localization of CYP19 in the mouse ovary showed that the MCL had a negative CYP19 reaction, whereas the immature corpus luteum revealed a weak reaction (**Figure 6A** and **6B**). The interstitial endocrine cells (IC) showed a negative reaction for CYP19 (**Figure 6A** and **6B**), whereas the preovulatory follicles showed an intense CYP19 reaction (**Figure 6A-D**). The average integrated densities of CYP19 in various parts of the ovary were markedly higher in the mature Graafian follicle, followed by the immature corpus luteum. The lowest values were detected in the primary and secondary follicles, MCL, and IC (**Figure 6E**).

IF localization of both 3β-HSD and RANK in the mouse corpus luteum showed a negative reaction for 3β-HSD but a positive reaction for RANK. The pre-antral follicle granulosa cells were negative for RANK and 3β-HSD, except in granulosa cells around the antral space (**Figure 7A-C**). Granulosa cells of the tertiary follicle revealed an intensely positive 3β-HSD reaction but a negative reaction for RANK, except at the follicle's periphery (**Figure 7D-F**). The IC showed a positive reaction for 3β-HSD and a negative reaction for RANK (**Figure 7D-F**). There were small follicles with weak reactions for both 3β-HSD and RANK (**Figure 7D-F**). The highest integrated densities of 3β-HSD were observed in the mature Graafian follicles and endocrine interstitial cells, followed by the immature corpus luteum and MCL, and finally the primary and secondary follicles (**Figure 7G**). The integrated density of

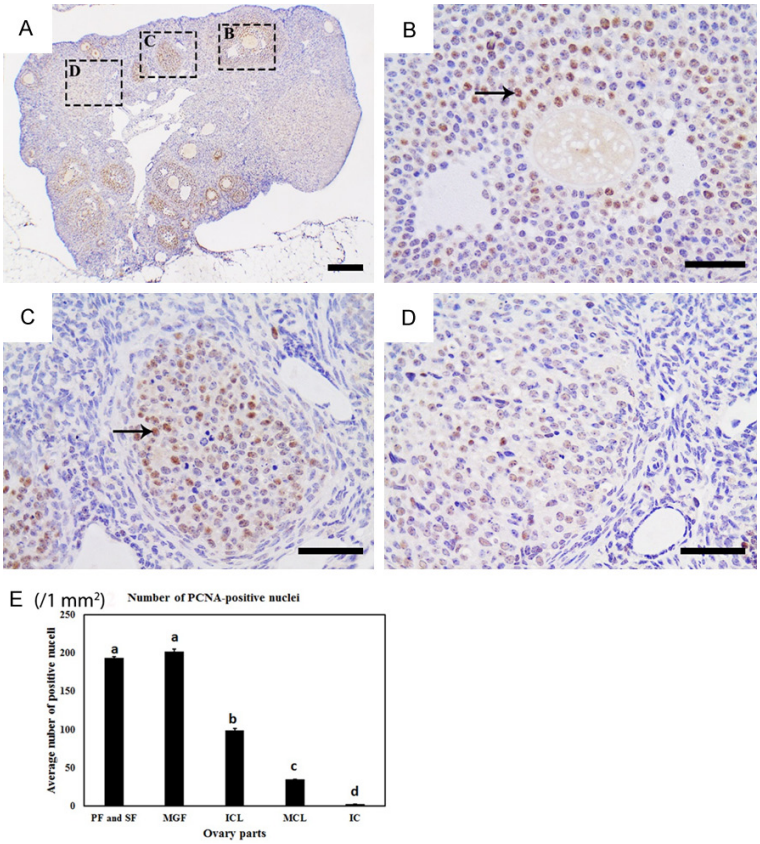


**Figure 4.** Distribution of proliferating cell nuclear antigen (PCNA)-immunopositive cells in the diestrus mouse ovary. (A) Immunohistochemical localization of PCNA showing the reaction of various parts of the ovary with PCNA. (B) The mature Graafian follicle, (C) immature corpus luteum, and (D) mature corpus luteum are insets of (A), revealing the high distribution of PCNA-immunopositive nuclei in the mature Graafian follicle and immature corpus luteum (arrows). Meanwhile, there was a very weak reaction in the mature corpus luteum. Scale bar = 200 μm. (E) The average number of PCNA-immunopositive nuclei per $mm^2$ for different parts of the ovary. Data are expressed as the mean ± SE. Bars with different superscripts are significantly different (Duncan's new multiple range test was used to compare the means among treatments; $P < 0.05$). PF, primary follicle; SF, secondary follicle; MGF, mature Graafian follicle; MCL, mature corpus luteum; ICL, immature corpus luteum; IC, interstitial cell.

RANK was the highest in the MCL, followed by the immature corpus luteum, but the lowest in mature Graafian follicles, IC, and primary and secondary follicles (**Figure 7H**).

The cellular localization of ER-α and calmodulin was determined using double IF in the mouse ovary. The results showed that the corpus luteum was moderately positive for ER-α and intensely positive for calmodulin (**Figure 8A-C**). Granulosa cells of the tertiary follicle revealed an intensely positive reaction for ER-α, whereas calmodulin showed a negative reaction, except at the follicle periphery (**Figure 8A-F**). The reaction of calmodulin occurred between ER-α-immunopositive cells (**Figure 8F** and **8I**). The lowest integrated densities of ER-α were detected in the mature Graafian follicles and IC, followed by the MCL (**Figure 8J**). The average integrated density of calmodulin was the highest in the MCL and mature Graafian follicles, followed by the immature corpus luteum, and the lowest in the endocrine interstitial cells and primary and secondary follicles (**Figure 8K**).

Double IF analysis of the PR and calbindin revealed a negative reaction for calbindin and a moderately positive reaction for PR in the corpus luteum (**Figure 9A-C**). The granulosa cells of the tertiary follicle were negative for calbindin and intensely positive for PR, but the oocyte showed a positive calbindin reaction. The granulosa cells of the secondary follicle showed positive reactions for both calbindin and PR. The cytoplasm of the secondary follicle oocytes was positive for calbindin, whereas the nucleus was positive for PR (**Figure 9D-F**). The immature corpus luteum was positive for both calbindin and PR. The IC were positive for PR, but negative for calbindin (**Figure 9D-F**). The lowest integrated densities of PR were detected in the mature Graafian follicles and IC, followed by the MCL (**Figure 9G**). Primary and secondary follicles had the highest integrated densities for calbindin, followed by mature Graafian follicles. The immature corpus luteum, MCL, and IC had the lowest integrated densities of calbindin (**Figure 9H**).

We found that CaSR was localized mainly in the tertiary follicle, but was not expressed in the corpus luteum (**Figure 10A** and **10B**). For the mature Graafian follicles, CaSR produced a positive reaction only with the oocyte plasmalemma (**Figure 10E** and **10F**). The average inte-

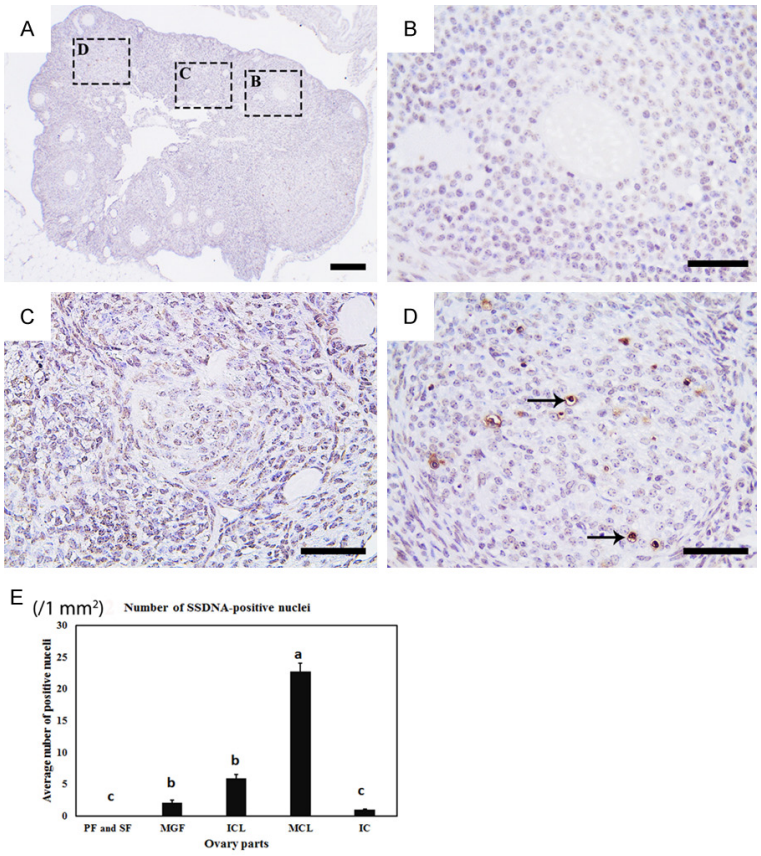


**Figure 5.** Distribution of single-stranded DNA (ssDNA)-immunopositive cells in the diestrus mouse ovary. (A) Immunohistochemical localization of ssDNA showing the reaction of different parts of the ovary with ssDNA. (B) The mature Graafian follicle, (C) immature corpus luteum, and (D) mature corpus luteum are insets of (A), revealing the high distribution of ssDNA-immunopositive nuclei only in the mature corpus luteum (arrows). Scale bar = 200 μm. (E) The average number of ssDNA-immunopositive nuclei per $mm^2$ for different parts of the ovary. Data are expressed as the mean ± SE. Bars with different superscripts are significantly different (Duncan's new multiple range test was used to compare the means among treatments; $P < 0.05$). PF, primary follicle; SF, secondary follicle; MGF, mature Graafian follicle; MCL, mature corpus luteum; ICL, immature corpus luteum; IC, interstitial cell.

grated density of CaSR was highest in the mature Graafian follicles, followed by the immature corpus luteum and primary and secondary follicles. The integrated densities of CaSR were the lowest in the MCL and interstitial cells (**Figure 10G**).

**Table 2** and **Figure 11** present the correlation coefficients of all study parameters. Notably, correlation analyses revealed moderate positive correlations between OBAP and SSDNA, 3β-HSD, and RNAK, but strong negative correlations with PCNA and calbindin. There was also a moderate negative correlation between OBAP and CaSR. Interestingly, aromatase CYP19 was positively correlated with 3β-HSD, ER-α, PR, calbindin, and CaSR. Meanwhile, ER-α showed a negative correlation with calbindin (**Table 2**).

## Discussion

In this study, we characterized the distribution of OBAP in the ovarian interstitial gland cells, oocytes, thecal cells of mature Graafian follicle, and lutein cells of the MCL. Moreover, the distribution of OBAP mostly showed an inverse relationship with PCNA levels in all ovarian compartments except oocytes. On the other hand, ssDNA levels revealed a positive relationship with OBAP distribution, except in the endocrine interstitial gland cells. The thecal, lutein, and interstitial gland cells in which OBAP was localized are steroid-secreting cells of the ovary [46]. Human chorionic gonadotropin can induce the secretion of cells of the endocrine interstitial gland, theca interna, and corpus luteum, but not granulosa cells [47]. Androgens are the steroids secreted by interstitial gland tissue [46], and theca interna cells are the primary androgen-secreting site of the ovary, with androgen being converted into estrogen by the granulosa cells of the mature Graafian follicle [48]. Therefore, the presence of OBAP in theca interna cells and interstitial gland cells could be attributed to the role of OBAP in androgen secretion.

In this study, PRα IF analysis revealed a moderately positive reaction in the MCL and an intensely positive reaction in the granulosa cells of secondary and tertiary follicles. Interestingly, OBAP-positive cells were distributed in the MCL, suggesting the correlation between OBAP and the secretion of the corpus luteum. Granulosa lutein cells, which are large cells derived from the granulosa, synthesize

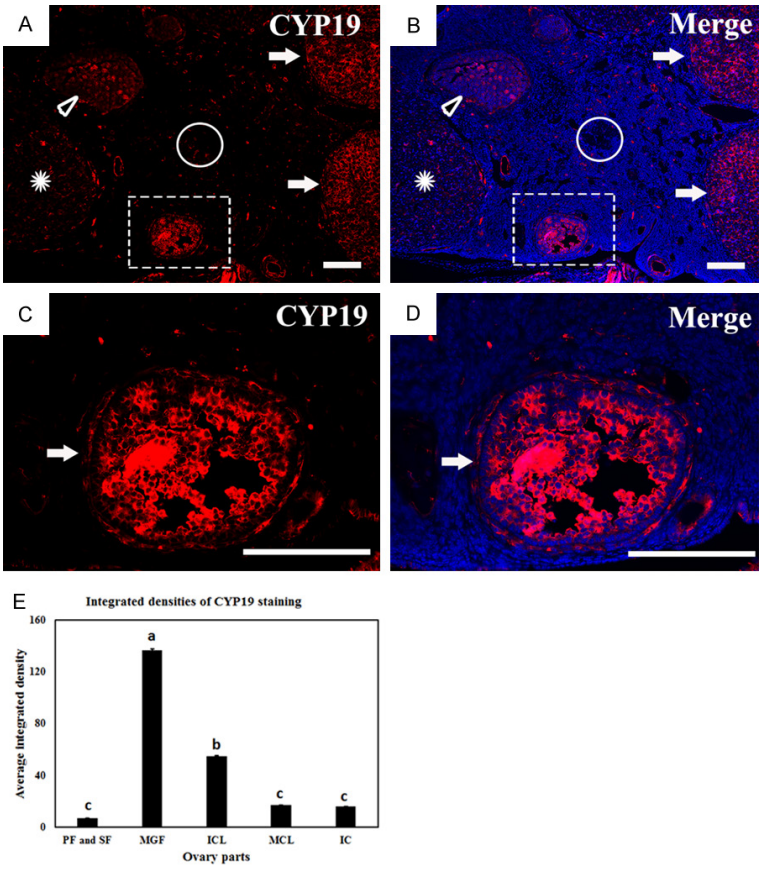


**Figure 6.** Immunofluorescence localization of aromatase (CYP19) (red) in the mouse ovary (A-D). In (A and B), the mature corpus luteum was negative for CYP19 (asterisks), whereas the immature corpus luteum showed a weak reaction (arrowheads). Interstitial endocrine cells were negative for CYP19 (circles). In (C and D), the preovulatory follicles showed an intense CYP19 reaction (thick arrows). Scale bar = 200 μm. (E) The average integrated densities of CYP19 staining for different parts of the ovary. Data are expressed as the mean ± SE. Bars with different superscripts are significantly different (Duncan's new multiple range test was used to compare the means among treatments; $P < 0.05$). PF, primary follicle; SF, secondary follicle; MGF, mature Graafian follicle; MCL, mature corpus luteum; ICL, immature corpus luteum; IC, interstitial cell.

progesterone and inhibin, whereas theca lutein cells secrete progesterone and androgens [48]. Seifert-Klauss and Prior [17] determined that progesterone prevents bone loss in peri- and premenopausal women because of the enhanced differentiation and proliferation of osteoprogenitor cells derived from adult females [19] and the anti-apoptotic effects of PRs [20], enhancing bone formation. Additionally, Christiansen, et al. [18] reported that elevated progesterone levels might be the main cause of low serum calcium. Therefore, OBAP and progesterone, secreted from the corpus luteum, may antagonize osteoblast apoptosis and reduce serum calcium levels, resulting in increased bone formation.

OBAP secretion was the lowest in the estrus phase and then increased gradually to reach its highest expression in the diestrus phase. Nielsen, et al. [49] detected a marked serum elevation of the osteoblastic bone markers osteocalcin and alkaline phosphatase during the metestrus and diestrus periods. These alterations suggested that osteoblastic activity is increased through these periods. An analysis of calcitonin levels revealed an elevation during diestrus and metestrus and a decrease during estrus [50]. Dullo and Vedi [12] detected the highest serum calcium level in the estrus phase and the lowest level in metestrus and diestrus, perhaps because of the effect of high estrogen secretion on the parathyroid glands during estrus [51] and higher levels of progesterone relative to estrogen during metestrus and diestrus [18]. Therefore, there may be a connection between calcitonin, OBAP, serum calcium, and osteoblast activity during the estrous cycle.

The development of the ovarian follicle in mice begins with the primordial follicle, which progresses to the mature Graafian follicle. Then, after ovulation, transformation to the corpus luteum occurs, followed by degeneration to form the interstitial endocrine gland cells from the theca lutein cells [52]. We used PCNA and ssDNA to investigate the relationship between OBAP positivity and ovarian follicle development in the context of proliferation and apoptosis. We noticed an inverse relationship between OBAP and PCNA. However, we found a positive relationship between OBAP and ssDNA reactions, except at the interstitial gland cells. Therefore, the relationship between OBAP and ovarian follicles could not be attributed to follicular development.

Our results clarified the negativity for the expression of CYP19 in the MCL and the IC, a

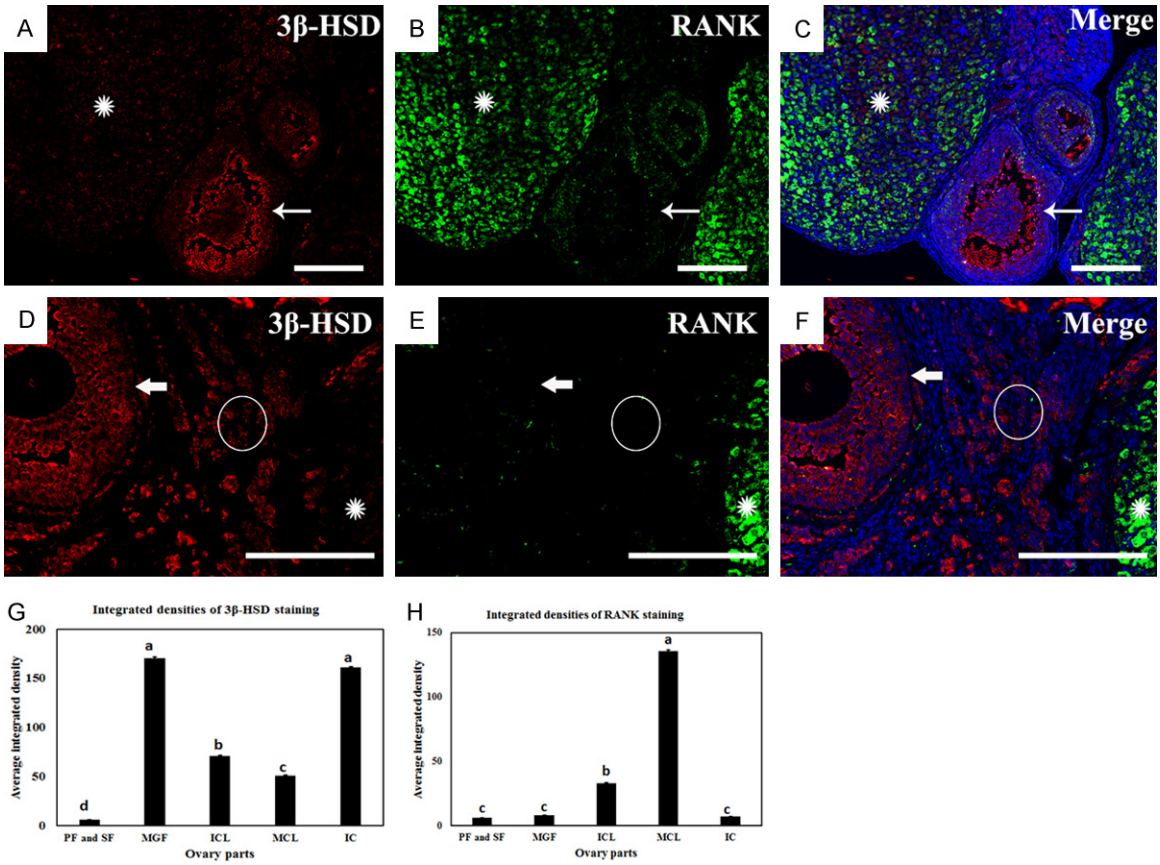


**Figure 7.** Immunofluorescence localization of 3β-HSD (red) and RANK (green) in the mouse ovary (A-F). In (A-C), the corpus luteum shows a positive reaction for RANK but a moderately positive reaction for 3β-HSD (asterisks). Granulosa cells of pre-antral follicle reveal a negative reaction for RANK and 3β-HSD, except for granulosa cells around the antral space (thin arrows). In (D-F), granulosa cells of the tertiary follicle reveal an intensely positive reaction for 3β-HSD (thick arrows), whereas RANK shows a negative reaction, except at the follicle periphery (thick arrows). Interstitial endocrine cells show a positive reaction for 3β-HSD but a negative reaction for RANK (circles). Scale bar = 200 μm. (G) The average integrated densities of staining for different parts of the ovary for 3β-HSD. (H) The average integrated densities of staining for different parts of the ovary for RANK. Data are expressed as the mean ± SE. Bars with different superscripts are significantly different (Duncan's new multiple range test was used to compare the means among treatments; $P < 0.05$). PF, primary follicle; SF, secondary follicle; MGF, mature Graafian follicle; MCL, mature corpus luteum; ICL, immature corpus luteum; IC, interstitial cell.

weak reaction in the immature corpus luteum, and an intense CYP19 reaction in the preovulatory follicles. This localization is inverse to that of OBAP expression in interstitial gland cells and the MCL. These findings are consistent with those reported by Ishimura, et al. [53]. Moreover, the granulosa cells of preovulatory follicles are the primary site of androgen to estrogen conversion, supplied by the interstitial gland cells and the theca interna cells [53]. Estrogen is produced in the ovary by progressive reactions mediated by several enzymes, including 3β-HSD and CYP19 [54]. The 3β-HSD enzyme is expressed within thecal cells surrounding follicles, whereas CYP19 is found within the granulosa cells inside follicles [55], indicating the cooperative actions of these distinct cell types in controlling estrogen synthesis. The interstitial gland cells in mouse ovaries are also steroidogenic, possessing functions like those of thecal cells [56]. This functional correlation of OBAP to steroidogenesis in the ovary is supported by the distribution of OBAP, which was reported to be enriched in ovarian steroidogenic interstitial gland cells [57].

The present study demonstrated the cellular localization of 3β-HSD in the mouse ovary, which showed a negative reaction for 3β-HSD in the corpus luteum. Marked immunoreactivity

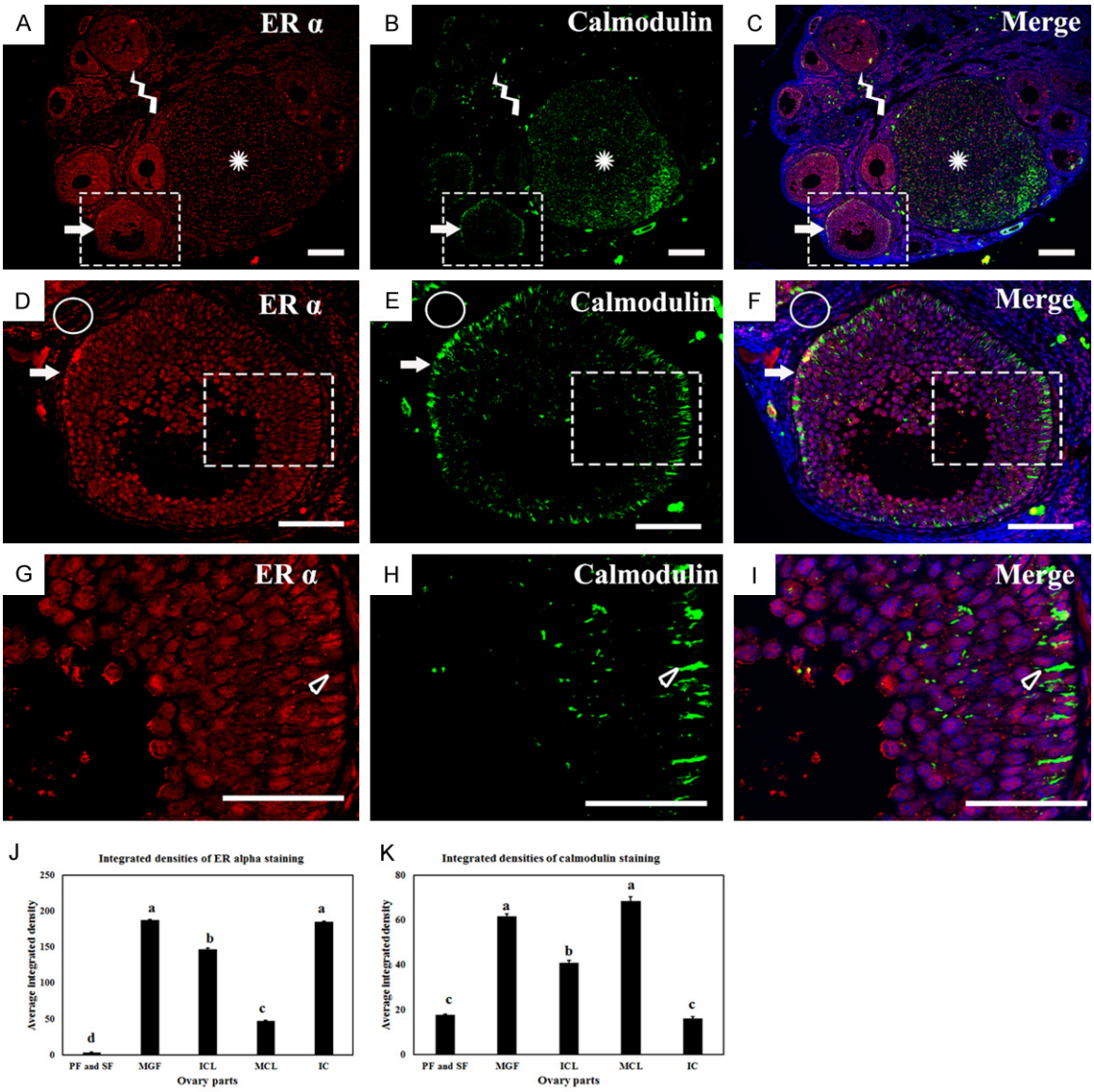


**Figure 8.** Immunofluorescence localization of estrogen receptor α (ER-α) (red; A, D, and G) and calmodulin (green; B, E, and H) in the mouse ovary. In (A-C), the corpus luteum reveals a moderately positive reaction for ER-α and an intensely positive reaction for calmodulin (asterisks). The immature corpus luteum shows positivity for ER-α and negativity for calmodulin (bent line). In (D-F), granulosa cells of tertiary follicle reveal an intensely positive reaction for ER-α, but a negative reaction for calmodulin, except at the periphery of the follicle (thick arrows). In (G-I), the reactivity for calmodulin is located between the ER-α-immunopositive cells (arrowheads). Scale bar = 200 μm. (J) The average integrated densities of staining for different parts of the ovary for ER-α. (K) The average integrated densities of staining for different parts of the ovary for calmodulin. Data are expressed as the mean ± SE. Bars with different superscripts are significantly different (Duncan's new multiple range test was used to compare the means among treatments; $P < 0.05$). PF, primary follicle; SF, secondary follicle; MGF, mature Graafian follicle; MCL, mature corpus luteum; ICL, immature corpus luteum; IC, interstitial cell.

was observed in luteinized thecal and granulosa cells of the corpus luteum [58]. The granulosa cells of the pre-antral follicle also revealed a negative reaction for 3β-HSD, except for granulosa cells around the antral space, whereas the granulosa cells of the tertiary follicle revealed intense positivity for 3β-HSD. The IC showed a positive reaction for 3β-HSD, which has been used as a marker for steroidogenic cells in the gonads [57]. Indeed, OBAP and 3β-HSD were detected immunohistochemically in the interstitial cells of the ovary. We observed

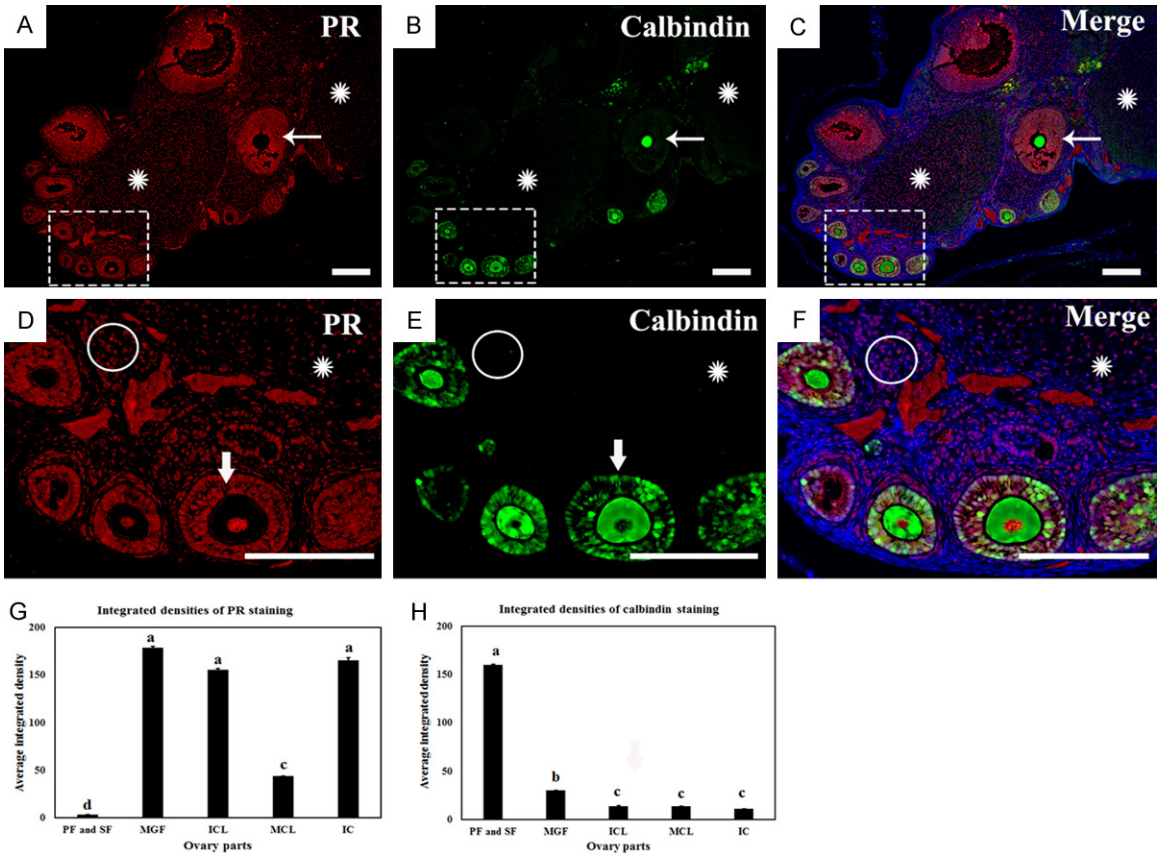


**Figure 9.** Immunofluorescence localization of progesterone receptor (PR) (red; A and D) and calbindin (green; B and E) in the mouse ovary. The corpus luteum was negative for calbindin and moderately positive for PR (asterisks). In (A-C), granulosa cells of tertiary follicle reveal a negative reaction for calbindin, but the oocyte shows a positive reaction (thin arrows). Granulosa cells of tertiary follicle reveal an intensely positive reaction for PR (thin arrows). In (D-F), Granulosa cells of the secondary follicle were positive for both calbindin and PR (thick arrow). The cytoplasm of the secondary follicle oocytes was positive for calbindin, whereas the nucleus was positive for PR (thick arrows). Interstitial endocrine cells show positivity for PR but negativity for calbindin (circles). Scale bar = 200 μm. (G) The average integrated densities of staining for different parts of the ovary for PR. (H) The average integrated densities of staining for different parts of the ovary for calbindin. Data are expressed as the mean ± SE. Bars with different superscripts are significantly different (Duncan's new multiple range test was used to compare the means among treatments; $P < 0.05$). PF, primary follicle; SF, secondary follicle; MGF, mature Graafian follicle; MCL, mature corpus luteum; ICL, immature corpus luteum; IC, interstitial cell.

3β-HSD only in the theca interna, but it became recognizable in the membrana granulosa with follicular development [58]. One to several layers of theca interna cells just beneath the membrana granulosa showed no immunoreactivity. These unstained theca interna cells did not appear to be directly involved in ovarian steroidogenesis and might be designated as enzymatically inactive theca interna cells [58]. Granulosa cell release of progesterone could be inhibited by troglitazone by the direct competitive inhibition of 3β-HSD [59].

Our results revealed that the pre-antral and tertiary follicle granulosa cells and the IC were RANK-negative. Meanwhile, the peripheral cells of the tertiary follicle and the corpus luteum were positive for RANK. RANK is a member of the TNF receptor family, which was initially discovered in a bone marrow-derived dendritic cell cDNA library. It plays an essential role in osteoclastogenesis and acts as a receptor for osteoclast differentiation factor [60]. Moreover, RANK is thought to facilitate the RANKL-mediated promotion of the survival of cultured dendritic cells [61]. The essential role of RANK in bone resorption was confirmed by studies in RANK-knockout mice, which showed a high bone mass phenotype and an almost complete lack of osteoclasts [62, 63]. RANK- and RANKL-knockout mice were virtual phenocopies of each other [62, 63], confirming that RANK and

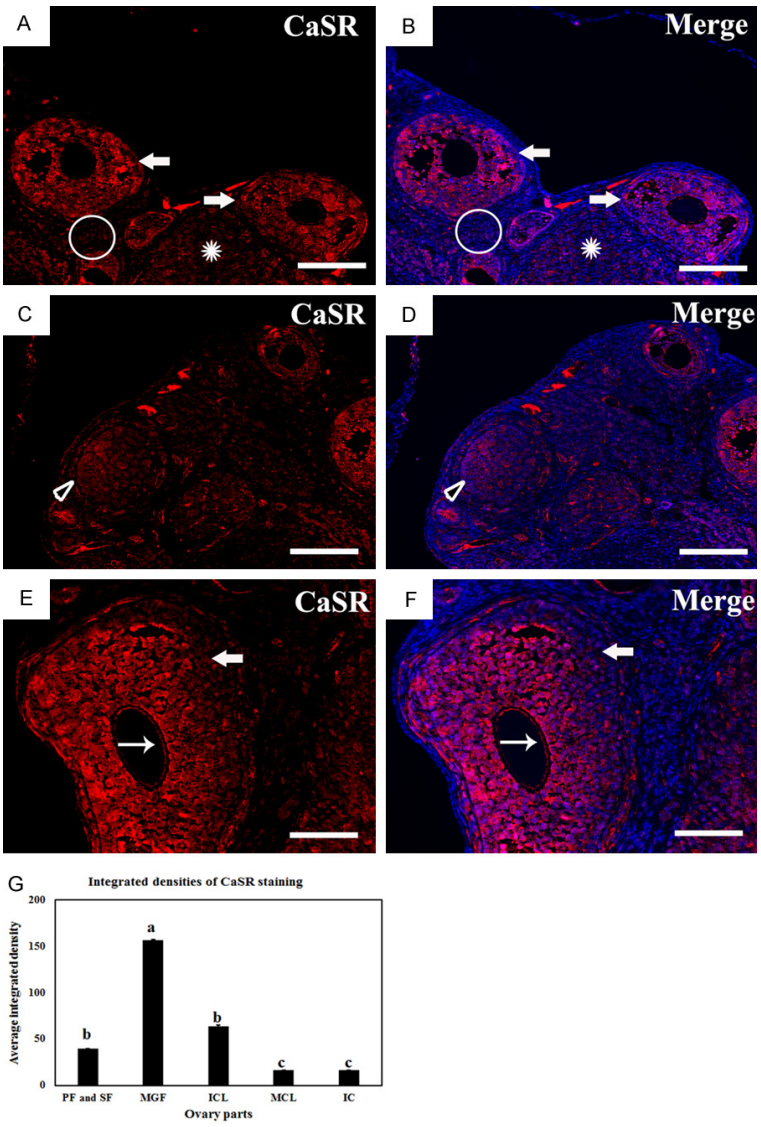


**Figure 10.** Immunofluorescence localization of the calcium-sensing receptor (CaSR) (red; A, C, E and merge; B, D, and F) in the mouse ovary. In (A and B), the mature corpus luteum reveals a weak CaSR reaction (asterisks), whereas the mature follicle shows an intense reaction (thick arrows). In (C and D), the immature corpus luteum reveals a weak CaSR reaction (arrowheads). In (E and F), CaSR reveals a positive reaction only with the plasmalemma of the oocyte (thin arrows). Interstitial endocrine cells were negative for CaSR (circles). Scale bar = 200 μm. (G) The average integrated densities of staining for different parts of the ovary for CaSR. Data are expressed as the mean ± SE. Bars with different superscripts are significantly different (Duncan's new multiple range test was used to compare the means among treatments; $P < 0.05$). PF, primary follicle; SF, secondary follicle; MGF, mature Graafian follicle; MCL, mature corpus luteum; ICL, immature corpus luteum; IC, interstitial cell.

RANKL have a minimal function beyond their mutual interaction.

Calmodulin is an essential protein that acts as a receptor to sense changes in calcium concentrations [64]. It is thought to regulate several intracellular processes, including cell proliferation, and act as an essential cell cycle regulator [65]. One of the most common mechanisms by which elevated intracellular calcium regulates cellular events is its association with calmodulin [66].

The cellular localization of ER-α and calmodulin in the corpus luteum showed a moderately positive reaction for ER-α and an intensely positive reaction for calmodulin. Granulosa cells of the tertiary follicle revealed an intensely positive reaction for ER-α, whereas calmodulin showed a negative reaction, except at the follicle periphery. Calmodulin reactivity was located between the ER-α-immunopositive cells. Calmodulin expression was also constant in the uterus, decidua, and placenta during different pregnancy stages, while other $Ca^{2+}$-binding proteins such as osteopontin and osteocalcin differed with the gestational stage [27].

Calbindin, a high-affinity calcium-binding protein, is regulated closely by 17β-estradiol and other steroid hormones, including 1,25-dihydroxyvitamin D3, glucocorticoids, and progesterone [67, 68]. In the present study, the MCL and granulosa cells of the tertiary follicle were negative for calbindin, but the oocyte was positive for calbindin. The granulosa cells of the secondary follicle showed positive reactions for both calbindin and PR. In oocytes of the secondary follicle, the cytoplasm was positive for calbindin, whereas the nucleus was positive for PR. The immature corpus luteum showed positive reactions for both calbindin and PR. The interstitial endocrine cells showed a posi-

**Table 2.** Correlation coefficient (r) between the examined parameters

| | OBAP | PCNA | SSDNA | CYP19 | 3β-HSD | ER alpha | PR | RANK | Calbindin | Calmodulin | CaSR |
|---|---|---|---|---|---|---|---|---|---|---|---|
| OBAP | 1 | | | | | | | | | | |
| PCNA | -0.897 | 1 | | | | | | | | | |
| SSDNA | 0.4189 | -0.448 | 1 | | | | | | | | |
| CYP19 | -0.312 | 0.4920 | -0.210 | 1 | | | | | | | |
| 3β-HSD | 0.4123 | -0.209 | -0.307 | 0.6116 | 1 | | | | | | |
| ER α | 0.2655 | -0.223 | -0.335 | 0.6118 | 0.9247 | 1 | | | | | |
| PR | 0.1859 | -0.180 | -0.319 | 0.6440 | 0.8799 | 0.992 | 1 | | | | |
| RANK | 0.4366 | -0.456 | 0.9951 | -0.2860 | -0.35 | -0.403 | -0.394 | 1 | | | |
| Calbindin | -0.623 | 0.6577 | -0.417 | -0.3024 | -0.620 | -0.701 | -0.705 | -0.353 | 1 | | |
| Calmodulin | 0.0890 | 0.0425 | 0.7125 | 0.5252 | 0.111 | 0.059 | 0.093 | 0.661 | -0.481 | 1 | |
| CaSR | -0.493 | 0.6800 | -0.336 | 0.9714 | 0.484 | 0.473 | 0.508 | -0.400 | -0.069 | 0.418 | 1 |

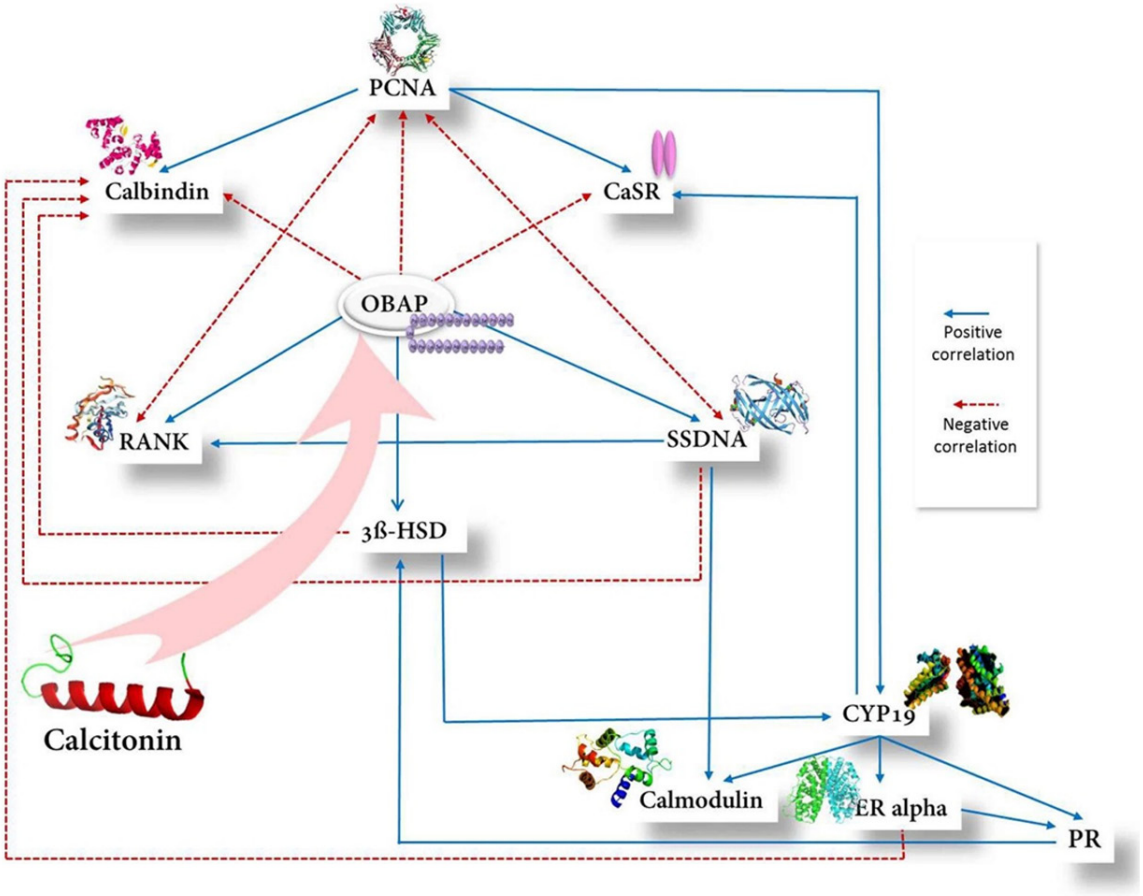


**Figure 11.** The proposed mechanism of action of OBAP in the local regulation of calcium signaling. Based on the correlation analysis, the interaction of calcitonin with OBAP is illustrated.

tive reaction for PR but a negative reaction for calbindin. The estrogen-responsive [69] and progesterone-responsive elements in the calbindin promoter mediate the transcriptional regulation of CaBP-28k in the rat uterus [70, 71]. Calbindin immunoreactivity was localized to the luminal epithelial cells of the fallopian tube of mature rats, with no staining observed in other tissue layers of the tube [72]. Calbindin-D28k may play a role in the transcellular movement of calcium across the fallopian tube epithelium in the fallopian tube lumen to regulate the

extracellular concentration of calcium needed for fertilization [72].

The current investigation showed that the CaSR was localized mainly in the tertiary follicle, but was not expressed in the corpus luteum. For the mature Graafian follicle, CaSR was detected only in the plasmalemma of the oocyte. $Ca^{2+}$ is the universal activator of development at fertilization, playing an essential role in early events, accompanied by a block of polyspermy, the egg-to-embryo transition, and egg activation by the completion of meiosis [73]. CaSR acts as a key mediator of cellular responses to physiologically relevant changes in extracellular $Ca^{2+}$ [33]. The distribution of OBAP in the oocyte ooplasm of the mature Graafian follicle and not in the primordial or primary follicle suggests the pivotal role of OBAP in oocyte maturation immediately before ovulation.

## Conclusions

In conclusion, we clarified that OBAP is expressed in a population of steroidogenic thecal and interstitial gland cells in adult mouse ovaries. It was positively correlated with ssDNA, calmodulin, and steroidogenic markers (ER, PR, 3β-HSD, and RANK), but had strong negative correlations with PCNA and aromatase (**Figure 11**). These findings suggest a possible role of OBAP in association with ovarian steroids and $Ca^{2+}$-binding proteins in regulating bone formation, bone remodeling, and osteoporosis and suggest a local role of OBAP in regulating calcium signaling in specific phases of the estrous cycle. Further mechanistic studies and the discovery of OBAP receptors are required to elucidate the possible relationship between OBAP and ovarian steroids and $Ca^{2+}$ homeostasis.

## Acknowledgements

A.E.N. was supported by a scholarship (No. 1-2013/2017) from the Egyptian Government.

## Disclosure of conflict of interest

None.

**Address correspondence to:** Islam M Saadeldin, Department of Physiology, Faculty of Veterinary Medicine, Zagazig University, Zagazig 44519, Egypt. Tel: +20552283683; E-mail: islamsaad82@gmail.com; islamms@zu.edu.eg

## References

[1] Ke H, Chen H, Simmons H, Qi H, Crawford D, Pirie C, Chidsey-Frink K, Ma Y, Jee W and Thompson D. Comparative effects of droloxifene, tamoxifen, and estrogen on bone, serum cholesterol, and uterine histology in the ovariectomized rat model. Bone 1997; 20: 31-39.

[2] Richards JB, Zheng HF and Spector TD. Genetics of osteoporosis from genome-wide association studies: advances and challenges. Nat Rev Genet 2012; 13: 576-588.

[3] Franzo A, Francescutti C and Simon G. Risk factors correlated with post-operative mortality for hip fracture surgery in the elderly: a population-based approach. Eur J Epidemiol 2005; 20: 985-991.

[4] Johnell O and Kanis JA. An estimate of the worldwide prevalence and disability associated with osteoporotic fractures. Osteoporos Int 2006; 17: 1726-1733.

[5] Rivadeneira F and Mäkitie O. Osteoporosis and bone mass disorders: from gene pathways to treatments. Trends Endocrinol Metab 2016; 27: 262-281.

[6] Black DM and Rosen CJ. Postmenopausal osteoporosis. N Engl J Med 2016; 374: 254-262.

[7] Andersson N, Surve VV, Lehto-Axtelius D, Ohlsson C, Håkanson R, Andersson K and Ryberg B. Drug-induced prevention of gastrectomy- and ovariectomy-induced osteopaenia in the young female rat. J Endocrinol 2002; 175: 695-703.

[8] D'Amelio P, Grimaldi A, Di Bella S, Brianza SZM, Cristofaro MA, Tamone C, Giribaldi G, Ulliers D, Pescarmona GP and Isaia G. Estrogen deficiency increases osteoclastogenesis up-regulating T cells activity: a key mechanism in osteoporosis. Bone 2008; 43: 92-100.

[9] Dick IM, Devine A, Beilby J and Prince RL. Effects of endogenous estrogen on renal calcium and phosphate handling in elderly women. Am J Physiol Endocrinol Metab 2005; 288: E430-435.

[10] Ranjzad F, Mahban A, Shemirani AI, Mahmoudi T, Vahedi M, Nikzamir A and Zali MR. Influence of gene variants related to calcium homeostasis on biochemical parameters of women with polycystic ovary syndrome. J Assist Reprod Genet 2011; 28: 225-232.

[11] Gallagher JC, Riggs BL and DeLuca HF. Effect of estrogen on calcium absorption and serum vitamin D metabolites in postmenopausal osteoporosis. J Clin Endocrinol Metab 1980; 51: 1359-1364.

[12] Dullo P and Vedi N. Changes in serum calcium, magnesium and inorganic phosphorus levels during different phases of the menstrual cycle. J Hum Reprod Sci 2008; 1: 77-80.

[13] Sakurada Y, Shirota M, Inoue K, Uchida N and Shirota K. New approach to in situ quantification of ovarian gene expression in rat using a laser microdissection technique: relationship between follicle types and regulation of inhibin-alpha and cytochrome P450aromatase genes in the rat ovary. Histochem Cell Biol 2006; 126: 735-741.
[14] Guigon CJ, Mazaud S, Forest MG, Brailly-Tabard S, Coudouel N and Magre S. Unaltered development of the initial follicular waves and normal pubertal onset in female rats after neonatal deletion of the follicular reserve. Endocrinology 2003; 144: 3651-3662.
[15] Turner KJ, Macpherson S, Millar MR, McNeilly AS, Williams K, Cranfield M, Groome NP, Sharpe RM, Fraser HM and Saunders PT. Development and validation of a new monoclonal antibody to mammalian aromatase. J Endocrinol 2002; 172: 21-30.
[16] Stocco C. Aromatase expression in the ovary: hormonal and molecular regulation. Steroids 2008; 73: 473-487.
[17] Seifert-Klauss V and Prior JC. Progesterone and bone: actions promoting bone health in women. J Osteoporos 2010; 2010: 845180-845180.
[18] Christiansen C, Riis BJ and Rodbro P. Prediction of rapid bone loss in postmenopausal women. Lancet 1987; 1: 1105-1108.
[19] Ishida Y and Heersche JN. Progesterone stimulates proliferation and differentiation of osteoprogenitor cells in bone cell populations derived from adult female but not from adult male rats. Bone 1997; 20: 17-25.
[20] Wang QP, Xie H, Yuan LQ, Luo XH, Li H, Wang D, Meng P and Liao EY. Effect of progesterone on apoptosis of murine MC3T3-E1 osteoblastic cells. Amino Acids 2009; 36: 57-63.
[21] Davey RA and Morris HA. Effects of estradiol and dihydrotestosterone on osteoblast gene expression in osteopenic ovariectomized rats. J Bone Miner Metab 2005; 23: 212-218.
[22] Westerlind KC, Wronski TJ, Ritman EL, Luo ZP, An KN, Bell NH and Turner RT. Estrogen regulates the rate of bone turnover but bone balance in ovariectomized rats is modulated by prevailing mechanical strain. Proc Natl Acad Sci U S A 1997; 94: 4199-4204.
[23] Kögl J, Wieser V, Sprung S, Fiegl H and Zeimet AG. EP891 Receptor activator of nuclear factor kappa-B ligand expression predicts ovarian cancer outcome. Int J Gynecol Cancer 2019; 29: A482-A483.
[24] Kearns AE, Khosla S and Kostenuik PJ. Receptor activator of nuclear factor κB ligand and osteoprotegerin regulation of bone remodeling in health and disease. Endocr Rev 2008; 29: 155-192.
[25] Hofbauer LC, Khosla S, Dunstan CR, Lacey DL, Spelsberg TC and Riggs BL. Estrogen stimulates gene expression and protein production of osteoprotegerin in human osteoblastic cells. Endocrinology 1999; 140: 4367-4370.
[26] Michael H, Härkönen PL, Väänänen HK and Hentunen TA. Estrogen and testosterone use different cellular pathways to inhibit osteoclastogenesis and bone resorption. J Bone Miner Res 2005; 20: 2224-2232.
[27] Waterhouse P, Parhar RS, Guo X, Lala PK and Denhardt DT. Regulated temporal and spatial expression of the calcium-binding proteins calcyclin and OPN (osteopontin) in mouse tissues during pregnancy. Mol Reprod Dev 1992; 32: 315-323.
[28] Belkacemi L, Züegel U, Steinmeyer A, Dion JP and Lafond J. Calbindin-D28k (CaBP28k) identification and regulation by 1, 25-dihydroxyvitamin D3 in human choriocarcinoma cell line JEG-3. Mol Cell Endocrinol 2005; 236: 31-41.
[29] Opperman LA, Saunders TJ, Bruns DE, Boyd JC, Mills SE and Bruns ME. Estrogen inhibits calbindin-D28k expression in mouse uterus. Endocrinology 1992; 130: 1728-1735.
[30] Inpanbutr N and Taylor A. Expression of calbindin-D28k in developing and growing ovaries of chicken embryos. Am J Vet Res 1993; 54: 514-519.
[31] Brown EM, Gamba G, Riccardi D, Lombardi M, Butters R, Kifor O, Sun A, Hediger MA, Lytton J and Hebert SC. Cloning and characterization of an extracellular Ca2+-sensing receptor from bovine parathyroid. Nature 1993; 366: 575-580.
[32] Chang W and Shoback D. Extracellular Ca2+-sensing receptors-an overview. Cell Calcium 2004; 35: 183-196.
[33] Rodland KD. The role of the calcium-sensing receptor in cancer. Cell Calcium 2004; 35: 291-295.
[34] Shoback D. Update in osteoporosis and metabolic bone disorders. J Clin Endocrinol Metab 2007; 92: 747-753.
[35] Fukushima N, Hiraoka K, Shirachi I, Kojima M and Nagata K. Isolation and characterization of a novel peptide, osteoblast activating peptide (OBAP), associated with osteoblast differentiation and bone formation. Biochem Biophys Res Commun 2010; 400: 157-163.
[36] Noreldin AE, Elewa YHA, Kon Y, Warita K and Hosaka YZ. Immunohistochemical localization of osteoblast activating peptide in the mouse kidney. Acta Histochem 2018; 120: 323-328.
[37] Noreldin AE, Sogabe M, Yamano Y, Uehara M, Mahdy MA, Elnasharty MA, Sayed-Ahmed A, Warita K and Hosaka YZ. Spatial distribution of osteoblast activating peptide in the rat stomach. Acta Histochem 2016; 118: 109-117.

[38] Schinke T, Schilling AF, Baranowsky A, Seitz S, Marshall RP, Linn T, Blaeker M, Huebner AK, Schulz A, Simon R, Gebauer M, Priemel M, Kornak U, Perkovic S, Barvencik F, Beil FT, Del Fattore A, Frattini A, Streichert T, Pueschel K, Villa A, Debatin KM, Rueger JM, Teti A, Zustin J, Sauter G and Amling M. Impaired gastric acidification negatively affects calcium homeostasis and bone mass. Nat Med 2009; 15: 674-681.

[39] Peng JB, Chen XZ, Berger UV, Vassilev PM, Brown EM and Hediger MA. A rat kidney-specific calcium transporter in the distal nephron. J Biol Chem 2000; 275: 28186-28194.

[40] McLean AC, Valenzuela N, Fai S and Bennett SA. Performing vaginal lavage, crystal violet staining, and vaginal cytological evaluation for mouse estrous cycle staging identification. J Vis Exp 2012; e4389.

[41] Bancroft JD and Layton C. The hematoxylin and eosin, connective and mesenchymal tissues with their stains. In: S. Kim suvarna CLaJDB, editor. Bancrofts Theory and practice of histological techniques. 7th, edition. Philadelphia Churchill Livingstone; 2013. pp. 173-186.

[42] Schneider CA, Rasband WS and Eliceiri KW. NIH Image to ImageJ: 25 years of image analysis. Nat Methods 2012; 9: 671-675.

[43] Onouchi S, Ichii O, Otsuka-Kanazawa S and Kon Y. Asymmetric morphology of the cells comprising the inner and outer bending sides of the murine duodenojejunal flexure. Cell Tissue Res 2015; 360: 273-285.

[44] SAS Institute. SAS/STAT procedure guide for personal computers. Cary, NC: SAS Institute; 1999.

[45] Petrie A and Watson P. Statistics for veterinary and animal science. John Wiley & Sons; 2013.

[46] Guraya SS. Recent advances in the morphology, histochemistry, biochemistry, and physiology of interstitial gland cells of mammalian ovary. International review of cytology. Elsevier; 1978. pp. 171-245.

[47] Falck B, Menander K and Nordanstedt OWE. Androgen secretion by the rat ovary. Nature 1962; 193: 593-594.

[48] Ross MH and Pawlina W. Female reproductive system. Histology a text and atlas with correlated cell and molecular biology. 7th, edition. Wolters Kluwer Health; 2016. pp. 824-875.

[49] Nielsen HK, Brixen K, Bouillon R and Mosekilde L. Changes in biochemical markers of osteoblastic activity during the menstrual cycle. J Clin Endocrinol Metab 1990; 70: 1431-1437.

[50] Cressent M, Elie C, Taboulet J, Moukhtar M and Milhaud G. Calcium regulating hormones during the estrous cycle of the rat. Proc Soc Exp Biol Med 1983; 172: 158-162.

[51] Pitkin RM, Reynolds WA, Williams GA and Hargis GK. Calcium-regulating hormones during the menstrual cycle. J Clin Endocrinol Metab 1978; 47: 626-632.

[52] Kelli B, Atis M, Mara HR, Rochelle LG and Katherine NG-C. Female reproductive system. In: Treuting PM, Dintzis SM, Montine KS, editors. Comparative anatomy and histology: a mouse, rat, and human atlas. Academic Press; 2017. pp. 303-334.

[53] Ishimura K, Yoshinaga-Hirabayashi T, Tsuri H, Fujita H and Osawa Y. Further immunocytochemical study on the localization of aromatase in the ovary of rats and mice. Histochemistry 1989; 90: 413-416.

[54] Martin M, Najera N, Garibay N, Malanco L, Martinez T, Rivera J, Rivera M and Queipo G. New genetic abnormalities in non-21α-hydroxylase-deficiency congenital adrenal hyperplasia. Sex Dev 2013; 7: 289-294.

[55] Chaffin CL and VandeVoort CA. Follicle growth, ovulation, and luteal formation in primates and rodents: a comparative perspective. Exp Biol Med (Maywood) 2013; 238: 539-548.

[56] Juneau C, Dupont E, Luu-The V, Labrie F and Pelletier G. Ontogenesis of 3β-hydroxysteroid dehydrogenase Δ5-Δ4 isomerase in the rat ovary as studied by immunocytochemistry and in situ hybridization. Biol Reprod 1993; 48: 226-234.

[57] Miyabayashi K, Tokunaga K, Otake H, Baba T, Shima Y and Morohashi KI. Heterogeneity of ovarian theca and interstitial gland cells in mice. PLoS One 2015; 10: e0128352.

[58] Sasano H, Mori T, Sasano N, Nagura H and Mason J. Immunolocalization of 3β-hydroxysteroid dehydrogenase in human ovary. J Reprod Fertil 1990; 89: 743-751.

[59] Gasic S, Nagamani M, Green A and Urban RJ. Troglitazone is a competitive inhibitor of 3β-hydroxysteroid dehydrogenase enzyme in the ovary. Am J Obstet Gynecol 2001; 184: 575-579.

[60] Nakagawa N, Kinosaki M, Yamaguchi K, Shima N, Yasuda H, Yano K, Morinaga T and Higashio K. RANK is the essential signaling receptor for osteoclast differentiation factor in osteoclastogenesis. Biochem Biophys Res Commun 1998; 253: 395-400.

[61] Anderson DM, Maraskovsky E, Billingsley WL, Dougall WC, Tometsko ME, Roux ER, Teepe MC, DuBose RF, Cosman D and Galibert L. A homologue of the TNF receptor and its ligand enhance T-cell growth and dendritic-cell function. Nature 1997; 390: 175-179.

[62] Dougall WC, Glaccum M, Charrier K, Rohrbach K, Brasel K, De Smedt T, Daro E, Smith J, Tometsko ME and Maliszewski CR. RANK is essen-

tial for osteoclast and lymph node development. Genes Dev 1999; 13: 2412-2424.
[63] Li J, Sarosi I, Yan XQ, Morony S, Capparelli C, Tan HL, McCabe S, Elliott R, Scully S and Van G. RANK is the intrinsic hematopoietic cell surface receptor that controls osteoclastogenesis and regulation of bone mass and calcium metabolism. Proc Natl Acad Sci U S A 2000; 97: 1566-1571.
[64] Klee C. Calcium as a cellular regulator. USA: Oxford University Press; 1999.
[65] Putkey J, Slaughter G and Means A. Bacterial expression and characterization of proteins derived from the chicken calmodulin cDNA and a calmodulin processed gene. J Biol Chem 1985; 260: 4704-4712.
[66] Means AR. Regulatory cascades involving calmodulin-dependent protein kinases. Mol Endocrinol 2000; 14: 4-13.
[67] An BS, Choi KC, Kang SK, Lee GS, Hong EJ, Hwang WS and Jeung EB. Mouse calbindin-D9k gene expression in the uterus during late pregnancy and lactation. Mol Cell Endocrinol 2003; 205: 79-88.
[68] Jung YW, Hong EJ, Choi KC and Jeung EB. Novel progestogenic activity of environmental endocrine disruptors in the upregulation of calbindin-D9k in an immature mouse model. Toxicol Sci 2005; 83: 78-88.
[69] Harvey PW and Everett DJ. Regulation of endocrine-disrupting chemicals: critical overview and deficiencies in toxicology and risk assessment for human health. Best Pract Res Clin Endocrinol Metab 2006; 20: 145-165.
[70] Lee KY, Oh GT, Kang JH, Shin SM, Heo BE, Yun YW, Paik SG, Krisinger J, Leung PC and Jeung EB. Transcriptional regulation of the mouse calbindin-D9k gene by the ovarian sex hormone. Mol Cells 2003; 16: 48-53.
[71] Darwish H, Krisinger J, Furlow JD, Smith C, Murdoch FE and DeLuca HF. An estrogen-responsive element mediates the transcriptional regulation of calbindin D-9K gene in rat uterus. J Biol Chem 1991; 266: 551-8.
[72] Mathieu CL, Mills SE, Burnett SH, Cloney DL, Bruns DE and Bruns ME. The presence and estrogen control of immunoreactive calbindin-D9k in the fallopian tube of the rat. Endocrinology 1989; 125: 2745-2750.
[73] Carvacho I, Piesche M, Maier TJ and Machaca K. Ion channel function during oocyte maturation and fertilization. Front Cell Dev Biol 2018; 6: 63.
[74] Strzalka W and Ziemienowicz A. Proliferating cell nuclear antigen (PCNA): a key factor in DNA replication and cell cycle regulation. Ann Bot 2011; 107: 1127-1140.
[75] Kawarada Y, Miura N and Sugiyama T. Antibody against single-stranded DNA useful for detecting apoptotic cells recognizes hexadeoxynucleotides with various base sequences. J Biochem 1998; 123: 492-498.
[76] Hishikawa Y, Damavandi E, Izumi S and Koji T. Molecular histochemical analysis of estrogen receptor alpha and beta expressions in the mouse ovary: in situ hybridization and Southwestern histochemistry. Med Electron Microsc 2003; 36: 67-73.
[77] Gava N, Clarke CL, Byth K, Arnett-Mansfield RL and deFazio A. Expression of progesterone receptors A and B in the mouse ovary during the estrous cycle. Endocrinology 2004; 145: 3487-3494.
[78] Duo X and Zhu WJ. Expression of the calbindin-d28k protein and gene in human ovary. J Reprod Contracept 2010; 21: 213-218.

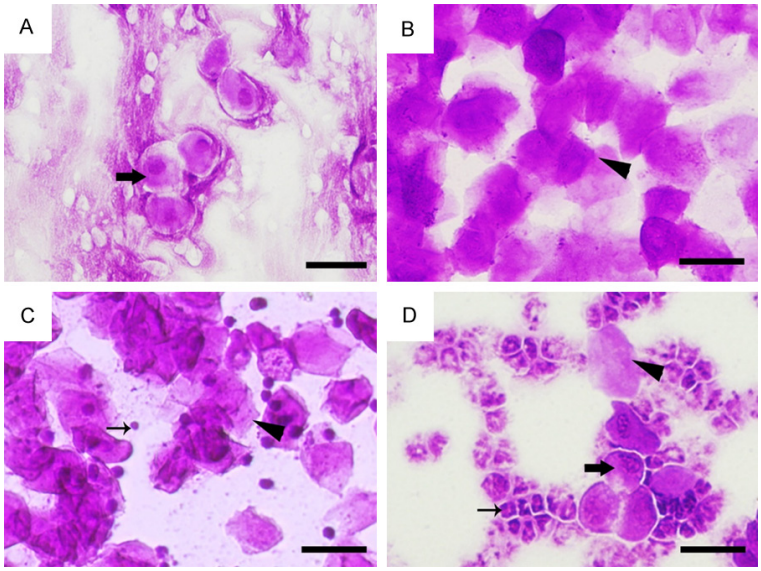


**Supplementary Figure 1.** Cytological assessment of mouse vaginal smears to identify the estrous cycle stages: (A) proestrus; (B) estrus; (C) metestrus; and (D) diestrus. Arrowheads in (B-D) refer to representative cornified squamous epithelial cells. Thin arrows in (C and D) refer to representative leukocytes. Thick arrows in (A and D) highlight representative nucleated epithelial cells. Scale bar = 50 μm.